

A&A manuscript no.
(will be inserted by hand later)

Your thesaurus codes are:
02.18.5; 02.19.2; 11.03.4: Coma; 11.09.3; 11.13.2

ASTRONOMY
AND
ASTROPHYSICS

Non-thermal Origin of the EUV and HEX Excess Emission of the Coma Cluster - the Nature of the Energetic Electrons

Torsten A. Enßlin¹, Richard Lieu², Peter L. Biermann¹

¹ Max-Planck-Institut für Radioastronomie, Auf dem Hügel 69, D-53121 Bonn, Germany

² Department of Physics, University of Alabama, Huntsville, AL 35899, USA
enßlin@mpifr-bonn.mpg.de, lieu@cspar.uah.edu, plbiermann@mpifr-bonn.mpg.de

Received ??? , Accepted ???

Abstract. The excess in extreme-ultraviolet (EUV) radiation and the recently discovered high energy X-ray (HEX) excess from the Coma cluster may be modeled using fewer parameters than in a thermal gas scenario, yet equally satisfactorily, by power law spectra. Their origin could therefore be inverse-Compton (IC) emission by relativistic electrons. The scattered background photon field can either be the cosmic microwave background (CMB) or the starlight of the elliptical galaxies within the cluster.

For the EUV excess both possibilities are consistent with the present data. If the EUV excess is due to CMB scattering, a strongly inhomogeneous magnetized intra-cluster medium (ICM) is required, in which the density of the IC scattering relativistic electrons is anticorrelated with the magnetic field. This could be understood if the electrons were accelerated during a major merger event within the last 2 Gyr and cooled afterwards in the inhomogeneous fields. If the EUV excess is due to scattered starlight, a population of relativistic, very low energy electrons has to be present, which would have a high energy density. In order to survive Coulomb losses, these electrons have to be separated from the dense thermal cluster gas by confining magnetic fields. Such a second component of the ICM could be remnant radio plasma left over from the epoch of violent quasar activity, which did not mix with the ICM. The observed narrow radial profile of the EUV excess emission is a natural consequence of this model due to the narrow profile of the photon distribution. Both models favor therefore very inhomogeneous magnetic field and relativistic electron distributions.

The IC models for the HEX excess require implausible conditions. CMB scattering leads to a mainly unmagnetized ICM, in contradiction to Faraday rotation measurements. Starlight IC scattering electrons would overproduce EUV photons due to simultaneously CMB scattering. We propose that the observed HEX excess is due to bremsstrahlung of a small high energy power-law tail of the mainly thermal ICM electron distribution. Such a

Key words: Radiation mechanism: non-thermal – Scattering – Galaxies: clusters: individual: Coma – Galaxies: intergalactic medium – Galaxies: magnetic fields

1. Introduction

The intra-cluster medium (ICM) of clusters of galaxies is known to consist of hot gas with temperatures of several keV. The gas is visible through the X-ray bremsstrahlung emitted by the hot electrons. Recent measurements in the spectral range below and above the thermal bulge show excess emission above what is expected from the thermal. This could indicate the presence of regions with different temperatures within the ICM, which could only be present there if the thermal conductivity is strongly reduced e.g. by tangled magnetic fields. But the excess emissions could also trace energetic non-thermal electrons via non-thermal radiation processes as bremsstrahlung and inverse Compton (IC) scattering of background photons.

We discuss three different non-thermal processes which could lead to the extreme ultraviolet (EUV) excess and the high energy X-ray (HEX) excess and their physical implications for the conditions within the ICM: In Sec. 2 the possibility that IC scattering of CMB photons is responsible for the observed excess emissions is examined. In Sec. 3 we describe a model for anisotropic IC scattering, as it has to be considered if the excess emissions are the scattered anisotropic starlight within the cluster. And in Sec. 4 non-thermal bremsstrahlung is proposed as an explanation of the HEX excess. In order to keep the discussion of the various IC processes as clear as possible, we concentrate on the EUV excess, and explain the consequences of the HEX excess for the different models in separate subsections. Sec. 5 contains a concise discussion of our results.

Parameters are estimated for $H_0 = 50 \text{ km s}^{-1} \text{ Mpc } h_{50}$,

region arcmin	spectral index	norm $10^{-3} \text{cm}^{-2} \text{s}^{-1} \text{keV}^{-1}$
0-3	$1.75^{+0.26}_{-0.18}$	$1.17^{+1.07}_{-0.58}$
3-6	$1.73^{+0.31}_{-0.16}$	$2.12^{+1.74}_{-1.15}$
6-9	$1.73^{+0.26}_{-0.16}$	$2.72^{+2.10}_{-1.36}$
9-12	$1.81^{+0.56}_{-0.25}$	$1.65^{+2.25}_{-1.16}$
12-15	$1.70^{+0.43}_{-0.19}$	$1.62^{+1.98}_{-1.06}$
15-18	$1.69^{+0.74}_{-0.22}$	$1.58^{+2.65}_{-1.28}$

Table 1. Results of the re-modeled EUV and soft X-ray data by Lieu et al. (1999). For the different angular rings the differential number index of the photon excess flux distribution, and the normalization (extrapolated flux at 1 keV) is given.

1.1. EUV Excess

The origin of the EUV excess observed in some clusters of galaxies (Coma, Virgo, Abell 1795, Abell 2199) is still under discussion. The first reports of this emission interpreted it in terms of a relatively cool component ($< \text{keV}$) of the hot ICM (Lieu et al. 1996a, 1996b; Bowyer et al. 1996, 1997; Mittaz et al. 1998). Doubts about the emission from cold gas were given by the nondetection of resonance lines by Dixon et al. (1996), expected in this case. An alternative explanation by inverse Compton (IC) scattered background light was proposed (Hwang 1997, Enßlin & Biermann 1998, Sarazin & Lieu 1998, Bowyer & Berghöfer 1998). The reader is referred to Sarazin & Lieu (1998) and Bowyer & Berghöfer (1998) for a broader discussion of the literature.

Recently, Lieu et al. (1999) re-modeled the soft excess in Coma with a power-law emission spectrum, and found satisfactory fits (reduced χ^2 between 1.10 and 1.36 for 180 degrees of freedom). Tab. 1 excerpts those aspects of their results relevant to this paper. The differential number index of the photon distribution is nearly independent of radius, so that we use a constant value of 1.75 for comparison with theoretical models. The spatial emission profile is narrow, and is plotted in Fig. 1 in comparison with the profile estimated by Bowyer and Berghöfer (1998), which is higher by 50%, and in comparison with the result of the starlight-IC model described in Sec. 3.

If IC scattering is the process producing the excess, as will be assumed in this paper, then relativistic electrons have to be present within the ICM. This is not surprising, since the Coma cluster is known to contain one of the largest radio halos (Willson 1970), and has therefore relativistic electrons in the energy range of (1.2 – 3.6) GeV $(B/(6 \mu\text{G}))^{-1/2}$, depending on the field strength B . The energy range of the electrons producing the IC emission can be estimated from the fact that electrons with momentum P scatter the peak of a thermal photon population

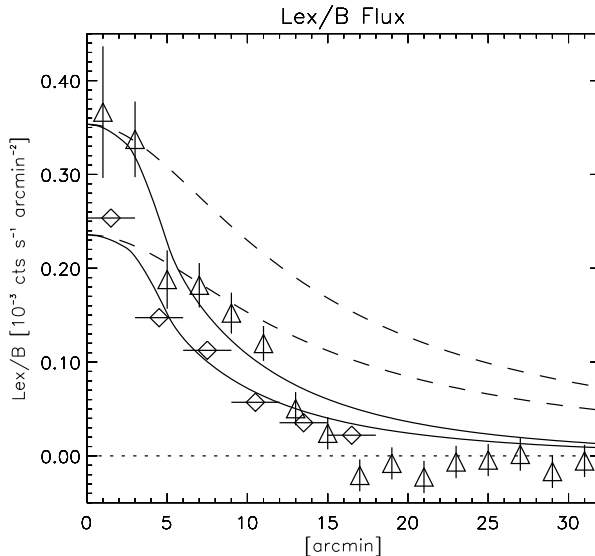


Fig. 1. Observed Lex/B excess flux from Bowyer and Berghöfer (1998) (triangles) and Lieu et al. (1999) (diamonds). The solid lines are the prediction of the anisotropic starlight-IC model of Sec. 3 for the two normalizations given there. The dashed lines are scaled projected electron profiles. The difference between the solid and dashed lines is due to the central enhancement in starlight photon density. The theoretical curves would be lower at larger radii, if the effect of enhanced IC scattering near galaxies exists as discussed in the Appendix. Note that the systematic uncertainties in the observed profile increases with radius due to the difficult data analysis.

fore that the electrons have momentum in the range 140 – 350 MeV/c. Another possibility is that the starlight of elliptical galaxies is scattered into the observational band (Enßlin & Biermann 1998). Since the temperature of this radiation field is roughly 3000 K, required electron momenta are in the range of only 4.4 – 10.6 MeV/c.

If it is possible to decide from physical consideration, which photon distribution is scattered into the EUV range and is observed, immediately information is given about a part of the relativistic electron spectrum below the radio range. The differential number index of the electron population in the energy range responsible for the emission has to be $\alpha_e = 2.5$, in order to produce an observed IC flux with photon differential number index of 1.75.

1.2. HEX excess

Early attempts to measure non-thermal HEX emission from the Coma cluster gave only upper limits, or inconsistent results (see Rephaeli et al. 1994 for upper limits

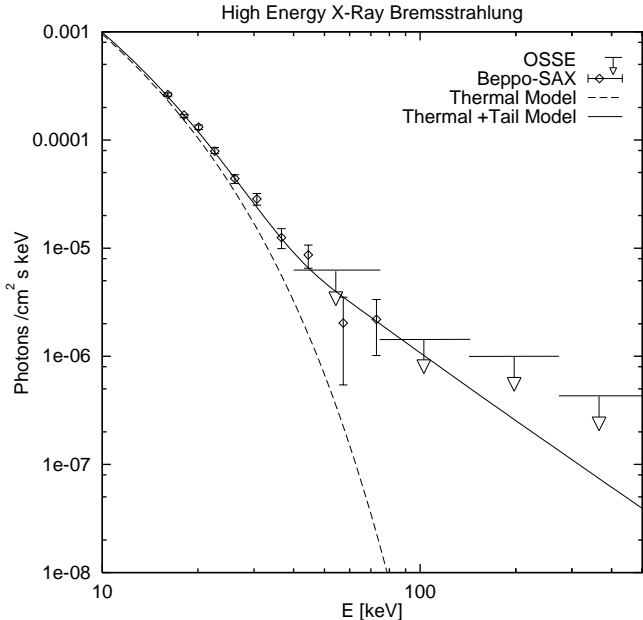


Fig. 2. HEX emission of Coma. The data points are from the Beppo-SAX measurement (Fusco-Femiano et al. 1998, 1999) and the upper limits from OSSE (Rephaeli et al. 1994). The lines are theoretical spectra, calculated in Sec. 4. The dashed curve belongs to a thermal electron distribution, and the solid curve if a non-thermal tail with number index $\alpha_e = 2.5$ is appended above a momentum of $P_e = 0.5 m_e c$ (or an kinetic energy of 60 keV).

above 25 keV, consistent with the OSSE upper limits. Assuming that the excess is due to a second thermal component would require a temperature of 40 keV for it (Fusco-Femiano et al. 1998, 1999), which seems to be implausible. The HEX spectrum is plotted in Fig. 2 in comparison with a thermal, and a modified thermal spectrum.

If the HEX is due to IC scattering of CMB photons, the necessary electrons would be within the energy range of 2.8–4.9 GeV, and therefore possibly visible at radio frequencies. In order to scatter starlight photons into the observed energy band, electrons between 84 and 150 MeV are needed. Fusco-Femiano et al. (1998) report that the HEX excess can be fitted satisfactorily with a power-law with photon number index of 0.97–3.45. The HEX excess flux is $2 \cdot 10^{-11} \text{ erg cm}^{-2} \text{ s}^{-1}$ between 20 and 80 keV, and within a radius of 1° . For comparison: An extrapolation of the EUV spectra (Tab. 1) to higher energies gives an excess flux between 20–80 keV of $1 \cdot 10^{-11} \text{ erg cm}^{-2} \text{ s}^{-1}$ within a radius of $18'$. Since the difference by a factor of two might be due to the larger field of view in the second case, a variation or a systematic error in the spectral indices or just a systematic effect in the estimate of

2. CMB-IC

2.1. Difficulties with the radio halo electrons

Hwang (1997) and Enßlin & Biermann (1998) discussed an inverse Compton model for the EUV excess in which the CMB photons are scattered by a population of relativistic electrons, which are the low energy tail of the population observed in the radio halo of Coma. This model is problematic for three reasons:

First, the spectral index of the radio emission is 1.16 (excluding some high frequency data point, Bowyer & Berghöfer 1998). Thus, the synchrotron emitting electrons have a differential number index of $\alpha_e = 3.32$, steeper than a CMB-IC scattering component with $\alpha_e = 2.5$. This means that a break has to be present in the electron spectrum at lower than radio emitting energies if both components belong to the same population. Giovannini et al. (1993) report a radial spectral index decrease of the radio halo. The central spectral index is 0.8 and the outer 1.8. The first corresponds to an electron number index of 2.6, which would be in good agreement with the required number index of the EUV producing electrons. Although this solves the first problem, it increases the difficulties with the magnetic field estimate as explained below.

Second, Bowyer and Berghöfer (1998) pointed out, that the radial profile of the EUV excess has a full width half maximum (FWHM) of 15.8 ($19.3 \times 12.6 \pm 1.5$). If the EUV excess is due to scattered CMB photons, the necessary electrons, which have energies of 140 – 350 MeV, have a profile with the same FWHM as the excess emission, whereas the low frequency radio profile has a much broader profile with a FWHM of $\approx 24'$. The strength of the radio emission, resulting from electrons with energies of $(1.2 - 3.6) \text{ GeV} (B/(6 \mu\text{G}))^{-1/2}$, is a product of the spatial densities of these electrons and B^2 (approximately). Since any reasonable profile of the magnetic fields should decrease with radius on the scale of a core radius, the spatial profile of these radio electrons has to be even broader than the radio emission itself, which is broader than the EUV emission. Thus, the FWHM of the electron population has to drop from a value which is considerably larger than $\approx 24'$ at 1 GeV (the radio range) to 15.8 at 350 MeV (CMB-IC scattering electrons). In other words, a low energy electron population which is spatially very differently distributed compared to the population producing the radio halo is required (Bowyer & Berghöfer 1998).

An extrapolating of the radial dependent radio spectra of Giovannini et al. (1993), would give an electron population at lower energies, which is less centrally concentrated as the radio population, due to the flat central spectral index. This is even more in conflict with the required compact spatial distribution of the EUV electrons.

Third, matching the distribution of the CMB scat-

the ICM is $\approx 1\mu\text{G}$, otherwise the total number of relativistic electrons would be too small in order to produce the EUV excess flux (Enßlin & Biermann 1998, Bowyer & Berghöfer 1998, see also Hwang 1997, who derives a volume averaged field strength of $0.4\mu\text{G}$). Since a spectral break is necessary between the regions of different spectral indices of radio- and IC-electron population, the allowed magnetic field strength is even lower than $1\mu\text{G}$.

The magnetic fields of the ICM can be independently measured by Faraday rotation of linear polarized radio emission traversing the ICM. The main uncertainty of this method is the underlying magnetic field reversal scale. A scale of $10\text{ kpc } h_{50}^{-1}$ gives a central field strength of $1.7 \pm 0.9\mu\text{G } h_{50}^{1/2}$ (Kim et al. 1990). But high resolution depolarization measurements indicate that the reversal scale is $1\text{ kpc } h_{50}^{-1}$ or below, leading to a ICM field strength of at least $6 \pm 1\mu\text{G } h_{50}^{1/2}$ (Feretti et al. 1995, but also predicted by Crusius-Wätzell et al. 1990). The field strength seems therefore to be higher than allowed by this IC model. The discrepancy between the field strength from Faraday rotation measurements and that from the synchrotron/IC ratio is solved,

- if there is a sharp step in the electron spectrum between the IC emitting electrons (140–350 MeV), and the radio emitting electrons (above 1 GeV), or
- if the medium is inhomogeneously magnetized on a small scale compared to the observational spatial resolution, and there is a strong anticorrelation between magnetic field strength and density of relativistic electrons – as Enßlin & Biermann (1998) proposed.

We demonstrate in the following, that for an electron population cooling in an inhomogeneously magnetized medium both are the case.

2.2. Merger events as a source of relativistic electrons

Such a population of electrons could initially be produced by shock acceleration during an energetic merger event in the past of Coma. Several such events should have happened, and there is evidence for recent and on-going events: Burns et al. (1995) propose that the X-ray emitting blob south-west of the center of Coma is due to the ascending motion of a group of galaxies around NGC 4839, which had a core passage 2 Gyr ago. Using kinematical considerations Colless & Dunn (1996) argue that this group is most probably infalling, therefore being in a pre- instead of post-merger stadium. Nevertheless these authors and others (Biviano et al. 1996, Vikhlinin et al. 1997, Donnelly et al. 1998) find apparent evidence for on-going or recent merger events in the cluster core from the galaxy velocity distribution and X-ray substructure. The time of injection of a relativistic electron population is expected

Synchrotron and inverse Compton cooling would lead to a cutoff in this distribution which evolves with time from higher to lower energies and would have reached 300 MeV after less than 1 Gyr for a magnetic field strength of $6\mu\text{G}$. After 1.5 Gyr it would be below 150 MeV (see Fig. 3). The injection of electrons which currently scatter the CMB into the EUV range should have happened less than 1 Gyr ago if the magnetic fields are homogeneous at $6\mu\text{G}$. But for inhomogeneous fields, and for an injection age of up to 2 Gyr sufficient electrons are still in this energy range, as will be demonstrated in the next section.

2.3. Cooling electrons in an inhomogeneous medium

A relativistic electron with dimensionless momentum $p = P_e/(m_e c)$ loses energy/momentum (Kardashev 1962) in the ICM at a rate of

$$-\frac{dp}{dt} = a_C + a_b p + a_s p^2. \quad (1)$$

The coefficient a_C , a_b , and a_s for Coulomb, bremsstrahlung, and synchrotron/IC losses are (Rephaeli 1979, Blumenthal & Gould 1970)

$$a_C = \frac{3}{2}\sigma_T c n_e \left(\ln \frac{m_e c^2 p^{1/2}}{\hbar \omega_p} + 0.22 \right), \quad (2)$$

$$a_b = \frac{3\alpha}{\pi}\sigma_T c n_e \left(\ln 2p - \frac{1}{3} \right), \quad (3)$$

$$a_s = \frac{4}{3}\sigma_T c \frac{\varepsilon_B + \varepsilon_{\text{cmb}}}{m_e c^2}, \quad (4)$$

where the electron density of the background gas is n_e , ε_B is the magnetic field and ε_{cmb} the CMB photon energy density. The plasma frequency is $\omega_p = \sqrt{4\pi e^2 n_e/m_e}$ and α is the fine-structure constant. a_C and a_b depend weakly on p , which we neglect in the following by inserting a typical value of $p = 10^3$ into the logarithms. We also use a density of $n_e = 3 \cdot 10^{-3}\text{ cm}^{-3} h_{50}^{1/2}$ (Briel et al. 1992) for the plasma frequency and in our following examples. Only a small error is introduced by using the constant p within the logarithms, but it allows an analytical calculation of the time dependent electron distribution. Further we assumed sufficiently fast pitch angle scattering of the electrons, so that the distribution can always be assumed to be isotropic, and Eq. 4 holds. The time needed to cool from p_0 to p_1 is given by an integration of Eq. 1

$$t_{\text{cool}}(p_0, p_1) = \frac{1}{a_s p_*} \left[\arctan\left(\frac{a_b}{2a_s p_*} + \frac{p_0}{p_*}\right) - \arctan\left(\frac{a_b}{2a_s p_*} + \frac{p_1}{p_*}\right) \right], \quad (5)$$

with

$$p_* = \frac{\sqrt{4a_s a_C - a_b^2}}{2a_s}, \quad (6)$$

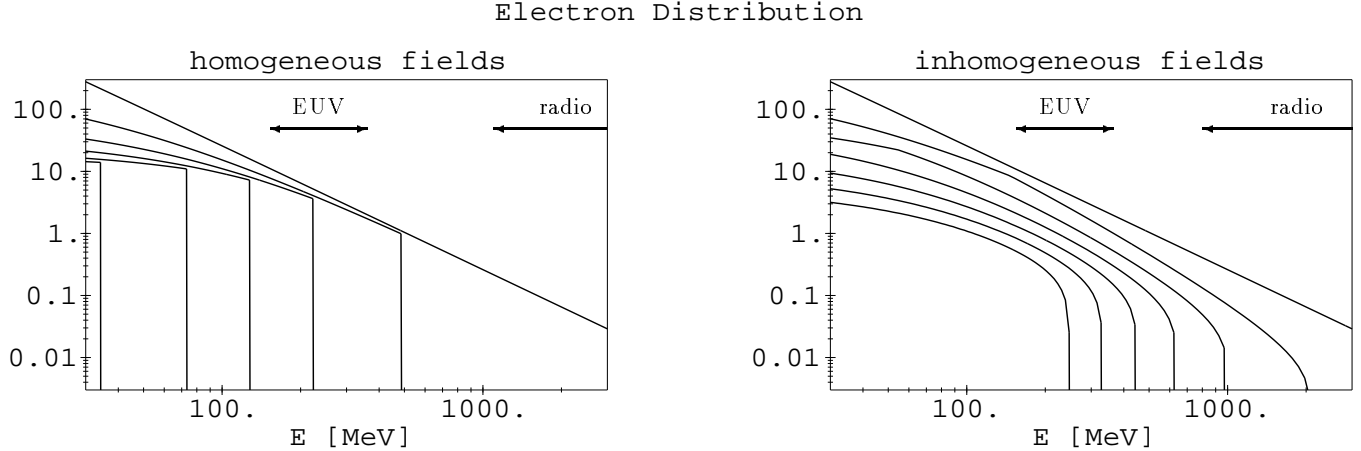


Fig. 3. Cooling electrons in a homogeneous magnetic field of $6 \mu\text{G}$ (left) and in inhomogeneous fields with mean field strength of $6 \mu\text{G}$ (right) ($\tilde{f}_e(p, t) dp$). In the latter case the average electron population is shown, averaged over the populations at different field strengths. The initial electron spectrum has a differential number index of 2 and is the highest curve. Plotted below this are electron populations after 0.5, 1, 1.5, 2, 2.5, and 3 Gyr of cooling. The energy ranges mainly responsible for the EUV excess emission by scattering of CMB photons and for radio emission are indicated. The different radio ranges result from different magnetic field strength distributions in these models. In the inhomogeneous model, the radio range has to be used with care, since the shown electron distribution is integrated over all regions with different field strength, but the radio range is shown for a field strength of $12 \mu\text{G}$.

This is 3 Gyr for a field strength of $6 \mu\text{G}$ and a gas electron density of $n_e = 3 \cdot 10^{-3} \text{ cm}^{-3}$. An electron with p_1 at the time t , had the initial momentum

$$p_0(p_1, t) = p_* \tan \left(a_s p_* t + \arctan \left(\frac{a_b}{2a_s p_*} + \frac{p_1}{p_*} \right) \right) - \frac{a_b}{2a_s}. \quad (8)$$

Thus, a population of relativistic electrons $f_{e,0}(p_0) dp_0$ which was injected at $t = 0$ into the ICM and which cooled afterwards without any additional acceleration has a time dependent distribution function, which is simply given by a transformation of the initial distribution under the mapping $p_0 \rightarrow p_1$

$$f_e(p_1, t) = f_{e,0}(p_0(p_1, t)) \frac{dp_0(p_1, t)}{dp_1} \quad (9)$$

as long as $t \leq t_{\text{cool}}(\infty, p_1)$, otherwise $f_e(p_1, t) = 0$.

In an inhomogeneously magnetized medium the spectrum of the cooling electrons becomes a function of position even in the case the initial spectrum was homogeneous due to the spatial dependence of the cooling. We suppose that there is no significant exchange of electrons between the different magnetized regions. This is a necessary condition in order to establish the required anticorrelation of magnetic fields and the electron population. It is also reasonable if the origin of the magnetic fields was injection by radio galaxies (Daly & Loeb 1990; Enßlin et al. 1997, 1998) or by galactic winds (Kronberg et al. 1999, but see also Völk et al. 1996 and Völk & Atoyan (1998) for the amount of non-thermal energy injected by galactic winds), since then the topology of the fields can be expected to

generated fields an inhomogeneous medium is also possible as the sun probably demonstrates.

Assuming a distribution of field strength $f_B(B) dB$ within a volume, which is sufficiently large compared to typical sizes of the magnetized regions, but small enough to be spatially unresolved by the current observations, we get a volume averaged electron population

$$\tilde{f}_e(p, t) = \int dB f_e(p, t, B) \quad (10)$$

where we wrote $f_e(p, t, B)$ instead of $f_e(p, t)$ in order to show explicitly the dependence of the local electron population on the local field strength. This averaged population is directly seen by the IC flux. Fig. 3 shows the volume averaged distribution function $\tilde{f}_e(p, t)$ for an injected distribution

$$f_{e,0}(p) = C_e p^{-2}, \quad \text{with } C_e = 10^6, \quad (11)$$

as one would expect after particle acceleration due to a strong shock wave in the ICM of a cluster merger event.

We assume a normalized distribution of magnetic fields $f_B(B) = 1/B_{\text{max}}$; for $0 \mu\text{G} < B < B_{\text{max}} = 12 \mu\text{G}$, (12)

and $f_B(B) = 0$ otherwise. This choice is arbitrary, but demonstrates well the effects we want to discuss. It leads to an averaged field strength of $6 \mu\text{G}$ consistent with Faraday rotation measurements. The electron population in a homogeneous field

$$f_B(B) = \delta(B - 6 \mu\text{G}) \quad (13)$$

is also shown in Fig. 3 for comparison.

The synchrotron emissivity at a given frequency ν of an

Synchrotron Spectrum

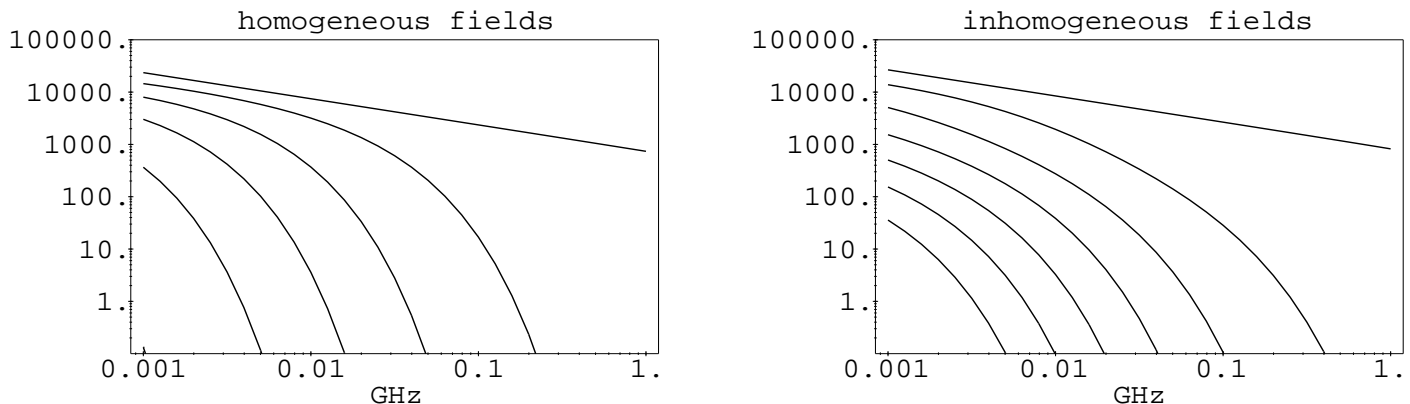


Fig. 4. Synchrotron emission of electron populations shown in Fig. 3 at an age of 0, 0.5, 1, 1.5, 2, 2.5, and 3 Gyr in units of $c_3 \mu\text{G} = 1.87 \cdot 10^{-29} \text{ erg s}^{-1} \text{ Hz}^{-1}$.

where $c_3 = \sqrt{3}e^3/(4\pi m_e c^2)$, $\nu_c(p, B) = 3eBp^2/(4\pi m_e c)$, and the angle averaged dimensionless spectral emissivity of a monoenergetic isotropic electron distribution (Crusius & Schlickeiser 1986) is

$$\tilde{F}(x) = \frac{\pi x}{2} \left(W_{0, \frac{4}{3}}(x) W_{0, \frac{1}{3}}(x) - W_{\frac{1}{2}, \frac{5}{6}}(x) W_{-\frac{1}{2}, \frac{5}{6}}(x) \right), \quad (15)$$

with $W_{\lambda, \mu}(x)$ denoting Whittaker's function (Abramowitz & Stegun 1965). $\tilde{F}(x)$ can be approximated to an accuracy of a few percent by

$$\tilde{F}(x) \approx \frac{2^{2/3}}{\Gamma(11/6)} \left(\frac{\pi}{3} \right)^{3/2} x^{1/3} \exp\left(-\frac{11}{8}x^{7/8}\right), \quad (16)$$

which is faster to evaluate numerically. Fig. 4 shows the synchrotron emission of a cooling population of electrons in the two models given above.

The important result of this simple inhomogeneous model is that the electron population in the weak field regions is still present in the energy range of 140 – 350 MeV after 2 Gyr of cooling, so that it can produce the EUV excess by IC scattering of CMB photons. But synchrotron/IC cooling produces a sharp cutoff at higher energies, so that for any given normalization of the electron population no observable radio emission remains. In the case of homogeneous fields a considerable amount of fine tuning of the time point of injection is necessary in order to allow a large electron population in the 140 – 350 MeV range, without overproducing low frequency radio emission, and therefore violating the observational constraints. As long as the magnetic fields are not lower than $6 \mu\text{G}$, the cooling time has to be near 0.6 Gyr, otherwise either the cutoff is lower than 400 MeV, or the electrons are visible in the radio.

An electron differential number index of 2.5 for the EUV producing energy range can easily be matched for sufficiently flat injection spectra. Unfortunately, the present day differential number index depends not only on

index of 2.15 would lead to a present day index of ≈ 2.5 in this energy range. If the field distribution is more strongly weighted to lower field strength, a steeper injection spectral index would be required, and if fewer low magnetic field regions exist a flatter one. With our poor present day knowledge about the distribution of field strengths it is therefore impossible to derive the injection spectrum.

The energy density of the relativistic electrons in the inhomogeneous model above after 2 Gyr is nearly two orders of magnitude smaller than the injected energy density, assuming that the injected spectrum extends from $P_e = 1 \text{ MeV}/c$ to $10^4 \text{ MeV}/c$, and the injection differential number index is 2.15. This energy loss depends strongly on the assumed distribution of fields: if more weak field regions are present the energy loss is much less dramatic. And since the present day population of EUV excess producing electrons has an energy density which is a factor of a few hundred below the thermal energy density (see Fig. 5. in Bowyer & Berghöfer 1998), an injection energy density considerably lower than the present thermal energy density would be sufficient to explain the present day EUV excess.

The effects of radius dependent electron and magnetic field distributions can in principle be treated with a similar formalism, where the volume average is then over elongated beams along the line of sight. Instead of giving a detailed model, which would rely on even more assumptions, we briefly discuss the qualitative behaviour. The magnetic fields strength and the injected electron energy density should decrease with radius. Due to the higher fraction of strong field regions in the center, one would expect a stronger cooling of the electrons there, and therefore a lack of energetic electrons there after a typical cooling time. But the fate of the low energy electrons, necessary for the CMB-IC EUV production, is mainly determined

is still varying with radius), then these electrons are still numerous in the cluster center.

2.4. In-situ accelerated electrons

Another possible origin of an electron population seen by CMB-IC is in-situ acceleration by plasma waves. A strong wave field can be expected if there is an on-going merger event in the center of Coma, as several authors (Colless & Dunn 1996, Biviano et al. 1996, Vikhlinin et al. 1997, Donnelly et al. 1998) report. The electron spectrum produced can be approximated by

$$f_e(p)dp = C_e p^{-\alpha_e} \exp\left(-\frac{p}{p_c}\right) dp \quad (17)$$

(Schlickeiser 1984), where the cutoff

$$p_c = \frac{v_A^2}{9a_s\kappa} \sim \frac{B^{2+\delta_\kappa}}{B^2 + 8\pi\varepsilon_{\text{cmb}}} \quad (18)$$

depends on the ratio of acceleration time scale to synchrotron/IC cooling time. v_A is the Alfvén velocity and $\kappa \sim B^{-\delta_\kappa}$ the spatial diffusion coefficient ($0 \leq \delta_\kappa \leq 1$). The cutoff p_c is a monotonically increasing function of the magnetic field strength, which implies that in the case of inhomogeneous fields the in-situ accelerated electron population reaches highest energies in the regions of strongest field strength. This is also supported by the more complicated dependence of α_e on the magnetic field strength: stronger fields result in harder spectra. The property of spatial anticorrelation between electron and magnetic field distributions, allowing a high number of radio quiet, low energy electrons, can therefore not be achieved within an in-situ acceleration model. In the case of inhomogeneous fields the in-situ acceleration model is more constrained than in the homogeneous case, due to the correlation of in-situ accelerated electrons and magnetic fields. But even for homogeneous fields the optimal parameters $\alpha_e = 1$, $p_c = 280$, which lead to an electron differential number index of 2.5 between 150 and 300 MeV/c, and which are still allowed by the theory of in-situ acceleration developed by Schlickeiser (1984), lead to an overproduction of synchrotron emission above 100 MHz for a field strength of 6 μG compared to the observations. The reason for this is the relative softness of the exponential cutoff of the electron population and the extended spectral width of the synchrotron emission.

We conclude that on-going in-situ acceleration is very unlikely the origin of a CMB-IC scattering electron population producing the EUV excess. This is astonishing in the light of evidence for merging activity in the cluster's center. It indicates that if merger events are responsible for the acceleration of energetic electrons, this happens only

2.5. Remaining difficulties of CMB-IC-EUV

The difficulty of a CMB-IC model for the EUV excess of Coma with the discrepancy between magnetic field strength observed by Faraday rotation, and the estimate using the IC- and synchrotron emission, can be overcome in a model where electrons cool in an inhomogeneous magnetic field. The narrow spatial emission profile is more difficult to understand within such a model, since one would expect a more extended electron distribution, in particular since the central electrons should cool faster than the peripheral ones. In order to decide, if this model is realistic or not, detailed simulations of the spatial distribution of electron acceleration during a merger core passage are required.

2.6. Difficulties of CMB-IC-HEX

Since the EUV and HEX excess fit roughly into a single power-law the HEX excess might also be produced by CMB IC scattering. The necessary electrons should be close to or within the energy range visible in the radio and therefore both populations have to be at least similar. Their cooling time due to synchrotron/IC losses is of the order of 10^8 years, so that continuous acceleration or very recent injection into this energy range is necessary. The observed HEX emission determines the number of electrons in the radio energy range, if one assumes the radio index also to be valid for the HEX producing electrons. In order to be in agreement with the observed synchrotron emission, the volume averaged magnetic fields strength has to be 0.16 μG (Fusco-Femiano et al. 1998, 1999), comparable to 0.4 μG given by Hwang (1997) for the EUV emission, which is energetically more distant to the radio range. The central magnetic field strength is roughly a factor of 3 higher, leading to $\approx 0.5 \mu\text{G}$, which seems to be too low in order to be consistent with the Faraday measurements of $6 \mu\text{G} h_{50}^{1/2}$.

Also for this 3–5 GeV electron population one might ask if (a) a sharp step in the electron spectrum, and (b) an inhomogeneous magnetized medium might resolve this discrepancy. The ICM needs to consist mainly out of regions with very weak fields (only a few 0.1 μG) containing the CMB IC scattering electrons, which are invisible in the radio due to the weak fields. But highly magnetized regions have to exist (maybe 10 μG or more), in order to explain the Faraday rotation, which need to contain only few 3–5 GeV electrons. If the difference in electron content of these regions was established by different cooling the time of injection had to be a few 0.1 Gyr in order to allow the several GeV electrons in the weak field regions still to be present, but those electrons living in the high field regions to have cooled to energies invisible in the ra-

let this model appear unsatisfactory. We conclude, that IC scattering of CMB photons as an explanation of the HEX excess seems to be implausible, unless there is something fundamental wrong with the Faraday rotation magnetic field estimates.

3. Starlight-IC

We propose a second model for the origin of the EUV photons, which has neither of the difficulties mentioned in Sec. 2.1: Inverse Compton scattering of starlight photons by very low energy relativistic electrons. This possibility was first mentioned by Enßlin and Biermann (1998), and used as a restriction on Coma's electron content in the energy range of a few MeV. The first, and third difficulties mentioned in Sec. 2.1 do not arise, since these electrons are energetically far away from the radio emitting range. The second one is also solved within this model, since in this case not only the electron population is centrally peaked, but also the target photon distribution, so that the emission profile can be narrower than the projected electron profile. For CMB-IC both profiles are the same since the CMB is uniform.

The cooling of electrons with a few MeV within the ICM is dominated by Coulomb losses and is so strong (cooling times ≤ 0.1 Gyr),

- (a) that it has to be compensated by efficient in-situ acceleration, or
- (b) that Coulomb losses have to be suppressed due to confining magnetic fields which contain the relativistic electrons, but not the dense thermal gas.

The latter might look a little bit artificial on a first view, but since a huge amount of relativistic plasma was injected into the ICM by radio galaxies in earlier epochs (Enßlin et al. 1997, 1998), a substantial part of this plasma might still be there as an unmixed, separate, nearly invisible, and non-thermal component of the ICM.

3.1. Anisotropic inverse Compton scattering

For a given spherical symmetric, radial source function $q_{\text{ph}}(r)$ of light emitted by galaxies, the photon density per volume and solid angle as a function of radius r and $\mu = \cos \theta$, the cosine of the angle between radial direction and photon direction, is given by a line integral backwards, over the line where these photons were emitted:

$$n_{\text{ph}}(r, \mu) = \frac{1}{4\pi c} \int_0^{s_{\text{max}}} ds q_{\text{ph}}(\sqrt{r^2 + s^2 - 2rs\mu}) \quad (19)$$

The maximal distance

$$s_{\text{max}} = \mu r + \sqrt{R_{\text{cl}}^2 - r^2(1 - \mu^2)} \quad (20)$$

is determined by the boundary of the cluster, which we assume to be $R_{\text{cl}} = 5 \text{ Mpc } h_{50}^{-1}$. The radial emission profile is

can be obtained by comparison with the observed central luminosity of elliptical galaxies in Coma, which we estimate by an integration of the R-band luminosity function of Secker & Harris (1996). We assume that this radiation has a blackbody spectrum with a typical temperature of 3000 K, and therefore use a bolometric correction of $m_{\text{R}} - m_{\text{bol}} = 1.3$ (Webbink & Jeffers 1969). We get a central luminosity of $9.3 \cdot 10^{12} L_{\odot} \text{ Mpc}^{-3} h_{50}$. Not included in this is the contribution of the two central giant elliptical galaxies NGC 4874 and NGC 4889. Their emission profile is of course not spherically symmetric with respect to the cluster center. Nevertheless we approximate their emission of $6.2 \cdot 10^{11} L_{\odot} h_{50}^{-2}$ (Strom & Strom 1978) to be homogeneously smeared out within a spherical shell between the radii of 100 and 200 kpc h_{50}^{-1} , since the present day EUV observations are not spatially resolved enough in order to justify the much higher computational effort a 3-dimensional model would require.

The distribution function of relativistic, low energy electrons is assumed to have spherical symmetry centered on the optical center of the cluster:

$$f_e(p, r) dp = C_{e,o}(r) g(p) dp = \frac{C_{e,o} p^{-\alpha_e} dp}{(1 + (r/r_{\text{core}})^2)^{\frac{3}{2}\beta}}, \quad (21)$$

with $C_{e,o} = 10^{-3} \text{ cm}^{-3} h_{50}$, which gives the right amount of IC photons estimated by Lieu et al. (1999), or $C_{e,o} = 1.5 \cdot 10^{-3} \text{ cm}^{-3} h_{50}$ in order to reproduce the EUV profile of Bowyer & Berghöfer (1998), which is higher by 50% but has a similar slope. Further we use $\alpha_e = 2.5$, $r_{\text{core}} = 400$ kpc, and $\beta = 0.75$, which are also the core radius and β -parameter of the background gas density (Briel et al. 1992). Such a profile¹ would be too narrow for the radio emitting electrons, but too wide for CMB-IC scattering electrons. But the profile of the very low energy starlight-IC electrons, which – together with the enclosing magnetic fields – would form a second component of the ICM, might be more similar to the global ICM gas profile than to that of the high energy radio electrons. On a small scale, we assume the gas and this non-thermal component to be separated.

The production density of IC scattered photons with energy higher than E_{ph} is

$$q_{\text{ICph}}(r, \mu, > E_{\text{ph}}) = \int_0^{2\pi} d\phi' \int_{-1}^1 d\mu' C_e(r) n_{\text{ph}}(r, \mu') \times \sigma(\mu', \phi', \mu) cF(> E_{\text{ph}}), \quad (22)$$

where ϕ' is the azimuth angle between the direction of the incident photon and the radial direction. The dependence on the azimuth angle ϕ of the scattered photon can be neglected due to symmetry. The anisotropic cross section of IC scattering by an isotropic power law distribution

¹ A gaussian profile $\sim \exp(-r^2/(700 \text{ kpc } h_{50}^{-1})^2)$, which is wider than the observed low frequency radio halo, and would be

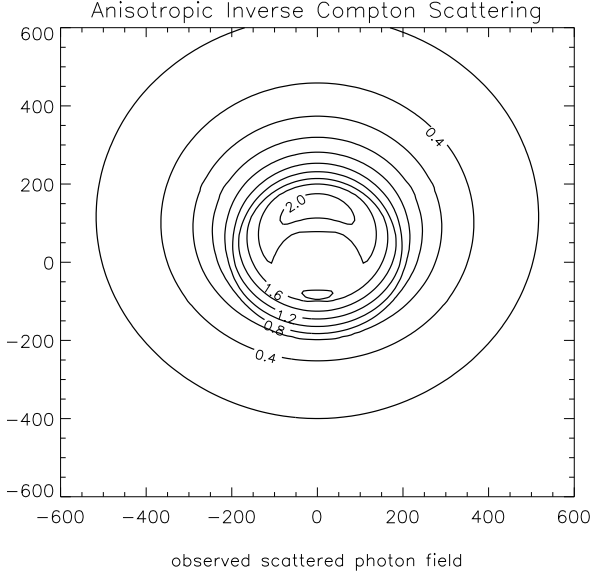


Fig. 5. Slice through the center of the Coma cluster. The emissivity into the direction of the observer, who is located downwards, is shown in units of 10^{-21} photons $\text{cm}^{-3} \text{s}^{-1} h_{50}$ within the energy band 69–400 eV, and with the normalization needed to fit the data of Lieu et al. (1999). The coordinates are given in $\text{kpc} h_{50}^{-1}$. The emission profile is not spherically symmetric due to the anisotropic efficiency of IC scattering by a steep electron spectrum with different scattering angle.

of electrons was derived by Brunetti et al. (1997). The anisotropy of the scattered photon field is mainly due to the fact, that for fixed initial and final (observed) photon energies the necessary electron energy depends on the scattering angle. Thus, for small-angle scattering a higher electron energy is necessary, which reduces the total number of scattering events due to the steepness of the electron spectrum. We use a crude approximation of the complicated expression given in Brunetti et al. (1997), which is sufficiently accurate for our purpose, especially for an electron number index of 3. This is close enough to the expected 2.5 so that the average deviation is less than 10 %:

$$\sigma(\mu', \phi', \mu) = \frac{3}{4} (\tilde{\mu}(\mu', \phi', \mu) - 1)^2 \sigma_T. \quad (23)$$

The cosine of the angle between incident and scattered photon is

$$\tilde{\mu}(\mu', \phi', \mu) = \cos \phi' \sqrt{1 - \mu'^2} \sqrt{1 - \mu^2} + \mu' \mu. \quad (24)$$

The spectral slope is given by the standard formula

$$F(> E_{\text{ph}}) = \frac{f_{\text{IC}}(\alpha_e)}{n_{\text{bb}}(k_B T)} \left(\frac{k_B T}{hc} \right)^3 \left(\frac{E_{\text{ph}}}{k_B T} \right)^{-\frac{\alpha_e - 1}{2}} \quad (25)$$

$$f_{\text{IC}}(\alpha_e) = \frac{3\pi 2^{\alpha_e + 4} (\alpha_e^2 + 4\alpha_e + 11)}{(\alpha_e + 3)^2 (\alpha_e + 5) (\alpha_e^2 - 1)} \Gamma\left(\frac{\alpha_e + 5}{2}\right) \zeta\left(\frac{\alpha_e + 5}{2}\right)$$

$k_B T$, introduced here for the proper normalization of the photon production rate. Fig. 5 shows a slice through the cluster center of the emission in the direction of the observer.

The observed scattered photon profile is the line of sight integration over the scattered photons

$$F_{\text{obs}}(R, > E_{\text{ph}}) = \int dz q_{\text{ICph}}(r(R, z), \mu(R, z), > E_{\text{ph}}), \quad (26)$$

with $r(R, z) = \sqrt{R^2 + z^2}$, and $\mu(R, z) = -z/r(R, z)$. The radius R in this formula can be translated via $l' \cong 39 \text{ kpc} h_{50}^{-1}$. We note that this anisotropic, line of sight integrated flux profile differs to one calculated assuming IC scattering to be isotropic. But our calculation shows that this difference is small.

Correcting for the spectral sensitivity of the Lexan-Boron filter of the Deep Survey Telescope of the EUV Explorer and the effect of Galactic absorption for $N_{\text{H}} = 8.7 \cdot 10^{19} \text{ cm}^{-2}$ (Lieu et al. 1996a), gives the theoretical predicted count rate, which is shown in Fig. 1 in comparison to the observed profiles and the slope of the assumed electron profile.

The IR-flux, produced by these electrons scattering the CMB photons, would be distributed as broad as the dashed lines in Fig. 1, and would be far below the present day limit on diffuse IR emission from Coma, as can be seen in Fig. 1 or Tab. 1 in Enßlin & Biermann (1998).

3.2. Energy density

The kinetic energy density of the assumed relativistic electron population ($C_{e,o} = 10^{-3} \text{ cm}^{-3} h_{50}$, Eq. 21) in the range of $P_e = 4.4 - 10.6 \text{ MeV}/c$ is $1.8 \cdot 10^{-10} \text{ erg cm}^{-3} h_{50}$ at the center of the cluster. This is more than the central thermal gas energy density of $1.2 \cdot 10^{-10} \text{ erg cm}^{-3} h_{50}^{1/2}$ (Briel et al. 1992). The ratio of the relativistic to thermal pressure is $0.8 h_{50}^{1/2}$ due to the smaller adiabatic index of the relativistic population. This seems to be very high, since one expects a similar pressure in confining magnetic fields and maybe in relativistic protons, which would be located at energies around 1 GeV due to their higher rest mass. Also the lower cutoff could be at a lower energy, which would increase the non-thermal energy density, too. If the low energy electrons are in-situ accelerated the energy density in turbulence has to be close to equipartition with the thermal energy density, as well. Although this is not ruled out, it looks very unlikely. The required amount of relativistic electrons could be lowered if

(a) important sources of optical photons were omitted. This could be e.g. a population of intra-cluster stars, tidally stripped from galaxies (Gregg & West 1998). Their light is not included in the luminosity function

- required relativistic electron energy density could be lowered only by up to 25–30%.
- (b) One might ask, if also IR- or UV-radiation fields of galaxies might give important contributions to the EUV flux. For an electron distribution with a single differential number index $\alpha_e = 2.5$, the contribution of a specific target population of photons with number density n_{ph} , and photon energy E_{ph} to the (fixed) observation band scales linearly with $E_{\text{ph}}^{(\alpha_e-1)/2} n_{\text{ph}} \sim E_{\text{ph}}^{0.75} n_{\text{ph}}$. Since the IR-, and UV- radiation fields have much lower energy densities than the optical photons, their contribution can be neglected.
- (c) The required energy can be strongly lowered if the correlation between electron density and starlight photon density is not only valid on a global cluster scale, as used in the above model, but also holds on the scale of individual galaxies, as should be demonstrated in the scenario described in the Appendix.

3.3. Difficulties of starlight-IC-HEX

Scattering of starlight into the HEX region in order to explain the observed excess needs a normalization constant of $C_{e,o} = 2 \cdot 10^{-4} \text{ cm}^{-3} h_{50}$ for $\alpha_e = 2.5$ and the β -model assumed above. Since the energy range of these electrons (84–150 MeV) overlaps with that of CMB-IC-EUV scattering electrons (140–350 MeV) both populations have to match. But the produced EUV emission would exceed the observed EUV excess by a factor of roughly 20. Unless starlight-IC enhancement (see Appendix) by a factor of 20 exists – which does not seem to be very likely – the starlight-IC model as the mechanism producing the HEX excess is ruled out.

4. HEX bremsstrahlung

The HEX-excesses is emission above what is expected for a thermal electron population. But the assumption of an exact thermal equilibrium might be questioned, since turbulence is present within clusters due to the stirring motion of galaxies, infalling subclumps, injection of radio lobes into the ICM, and streaming motion of the ICM itself, e.g. in cooling flows. This turbulence drags electrons out of the thermal tail, whenever they get into resonance with plasma waves, and accelerate them to higher energies. This leads to a modification of the distribution function so that the high energy cutoff of a thermal distribution is replaced by some power-law like region.

Further, since it is known from the radio halo that a relativistic population of electrons exists, there could be a spectral connection between relativistic and thermal populations: the electrons cooling from relativistic energies into the thermal population can add a power-law tail to

tion of the electrons. The EUV emission, which is energetically below the thermal bulge, can of course not be explained in this way.

The thermal electron distribution with temperature $k_{\text{B}}T = 8.21 \text{ keV}$ (Hughes et al. 1993) can be written as a trans-relativistic Maxwell-Boltzmann distribution in the dimensionless momentum $p = P_e/(m_e c)$

$$f_{e,\text{th}}(r, p) dp = \frac{n_{e,\text{th}}(r) \beta_{\text{th}}}{K_2(\beta_{\text{th}})} p^2 \exp(-\beta_{\text{th}} \sqrt{1+p^2}) dp, \quad (27)$$

with K_ν denoting the modified Bessel function of the second kind (Abramowitz & Stegun 1965), introduced here for proper normalization, $\beta_{\text{th}} = m_e c^2/k_{\text{B}}T$ the normalized thermal beta parameter, and

$$n_{e,\text{th}}(r) = n_{e,o} (1 + (r/r_c)^2)^{-\frac{3}{2}\beta} \quad (28)$$

the number density of thermal electrons, parametrized with the usual β -profile: $n_{e,o} = 2.89 \cdot 10^{-3} \text{ cm}^{-3} h_{50}^{1/2}$, $\beta = 0.75$, and $r_c = 400 \text{ kpc} h_{50}^{-1}$ (Briel et al. 1992). We add a power-law tail to this by writing

$$f_e(r, p) dp = \left\{ \begin{array}{ll} f_{e,\text{th}}(r, p); & p \leq p_* \\ C_e(r) p^{-\alpha_e}; & p > p_* \end{array} \right\} dp, \quad (29)$$

where the normalization parameter is determined from the condition of a smooth matching of the non- and thermal part to be $C_e(r) = p_*^{\alpha_e} f_{e,\text{th}}(r, p_*)$.

Assuming for illustration a number index of $\alpha_e = 2.5$, and choosing $p_* = 1/2$, which corresponds to a kinetic energy of $E_* = 60 \text{ keV}$, thus far above the typical thermal energy of 8 keV, gives $C_e(r) = 1.08 \cdot 10^{-2} n_{e,\text{th}}(r)$, or $C_e(0) = 3.13 \cdot 10^{-5} \text{ cm}^{-3} h_{50}^{1/2}$. This implies, that the total number in electrons is only increased by less than 1.8 %, even if the power law is extended to infinity. The kinetic energy density increases by less than 80 %, or by only 12 % if a higher cutoff is introduced at $p = 1$, which corresponds to a kinetic energy of 210 keV, sufficiently high in order to produce the observed emission up to 80 keV.

The bremsstrahlung emissivity spectrum is calculated via

$$q_{\text{X}}(r, k) dk = n_e(r) \int_0^\infty dp f_e(r, p) v(p) \sigma_{\text{X}}(p, k) dk, \quad (30)$$

where k is the photon momentum in units of $m_e c$, $v(p)$ the electron's velocity, and $\sigma_{\text{X}}(p, k) dk$ is the bremsstrahlung cross-section. We use the transrelativistic interpolation formula, and the Elwert factor given in Haug (1997) for a hydrogen plasma. Integrating this over the emission volume within 1° radius (or using the central emissivity times an emission weighted volume of $0.36 \text{ Mpc}^3 h_{50}^{-3}$), and redshifting the spectrum, gives the observed flux, which agrees well with the observed one, as can be seen in Fig. 2.

The above assumed parameter $\alpha = 2.5$ and $p_* = 1/2$ (corresponding to $E_* = 60 \text{ keV}$) reproduce the BeppoSAX and OSSE data with a χ_{red}^2 of 1.6. A systematic χ_{red}^2 estimate is shown in Fig. 6. The absolute minimum is at $\alpha = 2.9$, and $E_* = 62.5 \text{ keV}$ with $\chi_{\text{red}}^2 = 0.86$. The length of the χ^2 -valley in Fig. 6 indicates that the necessary

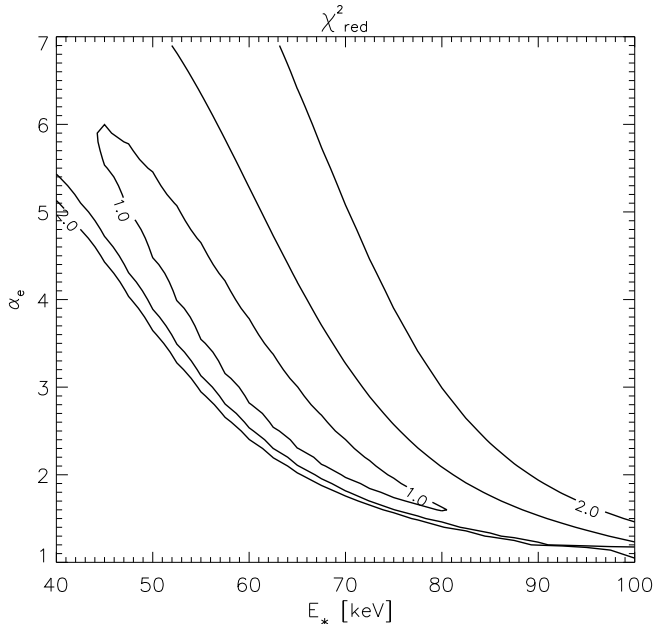


Fig. 6. χ_{red}^2 for the bremsstrahlung model described in the text plotted for E_* the matching energy of the power-law and thermal electrons, and α_e the spectral index of the former. The OSSE and Beppo-Sax data is used simultaneously.

spectrum can be expected, if in-situ acceleration produces this tail by accelerating thermal electrons against the fast Coulomb cooling, which has a cooling time of $t_C \approx 10^5$ yr for 60 - 100 keV electrons (Spitzer 1968). Also models with a high energy cutoff anywhere above 100 keV in the power-law tail give satisfactory χ_{red}^2 .

5. Discussion

5.1. EUV excess

We discussed two inverse Compton processes, which could explain the power law EUV excess of clusters of galaxies at the example of the Coma cluster.

The first one is IC scattering of the CMB. This requires a sharp cutoff in the electron distribution above the relevant energy range of 140–350 MeV, otherwise the electrons above this range overproduce low frequency radio emission. In-situ acceleration produces an exponential cutoff, too soft to hide this electron component. We propose that the relativistic electrons were accelerated by a shock wave during a merger event of Coma, up to 2 Gyr ago. Synchrotron and IC cooling produces a sharp cutoff in the energy spectrum. In order to allow electrons to be still within the EUV producing energy range after a cooling time of 2 Gyr, regions of lower than average magnetic fields are necessary within the ICM, which is a natural

event can show that the resulting accelerated electron profile is indeed as narrow as required.

The second model is IC scattering of starlight photons by electrons in the energy range of 4–10 MeV. Since the target photon distribution is peaked at the center of the cluster, the profile of the scattered photons is narrower than that of the electrons. In order to establish such an electron population, which would have a pressure similar to that of the thermal background gas (but see Appendix for the possibility of a much lower pressure), confining magnetic fields have to separate these electrons from the dense thermal background gas in order to prohibit the strong Coulomb losses. This may be the case within remnant radio plasma from early epochs of quasar activity, which did not mix with the gas, and which can form a second, nearly invisible, non-thermal component of the ICM. Future high resolution EUV observations may be able to resolve the possible enhanced IC emission near the giant elliptical galaxies in Coma as it would be expected in the starlight IC model. Since the starlight-IC model does not require a sharp cutoff above the IC emitting electrons, IC flux of higher energy than the thermal X-ray emission could be expected. A high non-thermal pressure in galaxy clusters was suggested to be a possible explanation of the discrepancy between hydrostatic and lensing masses of clusters (Loeb & Mao 1994, Miralda-Escudé & Babul 1995, Enßlin et al. 1997)

5.2. HEX excess

Both IC processes discussed above lead to unsatisfactory implications for the ICM, if they were considered as the explanation of the HEX excess:

IC scattering of CMB photons requires the ICM to be mainly unmagnetized ($B \ll \mu\text{G}$), in order to avoid an overproduction of synchrotron emission by the scattering electrons. But in order to be in agreement with current measurements of ICM Faraday rotation, regions with strong field strength ($B \gg \mu\text{G}$), but without a significant population of 3–5 GeV electrons have to be present. This spatially very different electron content could be due to spatially differentiated cooling, but only if no intermediate magnetized regions ($B \approx \mu\text{G}$) exist in the ICM, otherwise the radio emission would be too strong. Further, the injection of the electrons had to be a few 0.1 Gyr ago, not more or less, since otherwise the strong field region still contains radio luminous electrons, or the unmagnetized regions lost their 3–5 GeV electrons due to IC-cooling.

The starlight IC model for the HEX excess requires a high electron number density in the energy range of 84–150 MeV, which is too close to the energies necessary to scatter the CMB photons into the EUV band as that an overproduction of EUV flux can avoided. Only if the

We propose a third explanation of the HEX excess, which is not in conflict with observations at other wave bands. Due to galactic motions, infall of subclusters, convective movement of the gas, etc., turbulence is present and therefore in-situ acceleration is expected to drag electrons out of the thermal distribution and to accelerate them. This might lead to a power-law like high energy tail of the distribution function above ≈ 50 keV. The HEX excess is satisfactorily explained by the bremsstrahlung of these electrons.

6. Conclusion

We conclude, that the EUV excess can be explained either with the CMB-IC model, which has the advantage of a low energy density in the required relativistic electrons, or with starlight-IC, which requires a high energy density, but explains naturally the observed narrow emission profile. The latter model would be supported if future observations with high spatial resolution discover a correlation between the location of luminous galaxies and the EUV flux. Both models favor a strongly inhomogeneous magnetized ICM. The electrons of 140–350 MeV required in the CMB-IC model should have aged after injection for up to 2 Gyrs within the inhomogeneous fields, in order to be consistent with radio constraints. This favors as an origin of these electrons shock acceleration during a past cluster merger. The origin of the 4.4-11 MeV electrons in the starlight-IC model is expected to be the radio plasma outflow of earlier radio galaxies. The CMB- and the Starlight-IC model do not exclude each other. Therefore a combined contribution is possible.

The HEX excess is most likely bremsstrahlung of a supra-thermal tail above 50 keV of the electron energy distribution, tracing acceleration and cooling processes of transrelativistic electrons.

Future observations, which extend the observed spectral range of these non-thermal excess emissions, and improve the spatial resolution, would give further important insight into the complex trans- and ultra-relativistic processes within the ICM, and its inhomogeneous structure.

Acknowledgements. We acknowledge very useful discussions with Thomas Berghöfer, Christian Zier, and Phil Kronberg. We thank Stuart Bowyer, Thomas Berghöfer, Roberto Fusco-Femiano, and his co-workers for giving us their data. This manuscript was considerably improved due to comments by an anonymous referee. TAE acknowledges support by the *Studienstiftung* and the MPIfR.

Appendix A: Enhanced starlight-IC

The transition between ICM and ISM of individual elliptical

than at the center of the cluster wide X-ray emission (Lazzati & Chincarini 1998). We model the background gas around a cluster galaxy by

$$X(r) = \frac{n_{e,\text{gal}}(r)}{n_{e,\text{cl}}} = 1 + \frac{X_o - 1}{1 + r^2/r_X^2}, \quad (\text{A.1})$$

where $n_{e,\text{cl}}$ is the background density of the ICM. X_o , which we assume in our example to be $X_o = 7$, is the maximal compression of the ICM density the galaxy achieves in its potential on a scale of r_X . The radius from the center of the galaxy is r .

First, we estimate the change of conventional observables due to this compression. The temperature increases by a factor of $X^{2/3}(r)$. The enhancement in X-ray emission is $X^{7/3}(r)$, since $L_X \sim n_e^2 T^{1/2}$. Averaging this over a typical volume a galaxy occupies within the cluster, which we tentatively assume to be a sphere with radius $10 r_X$, one gets an increased emissivity by a factor of 1.5 over the same volume filled by background gas. An estimate of the background gas properties, assuming a homogeneous medium and using the observed X-ray data, should result in a (emission weighted) gas density and temperature of $1.16 n_{e,\text{cl}}$ and $1.21 T_{\text{cl}}$, only moderately different from the background values $n_{e,\text{cl}}, T_{\text{cl}}$.

The population of relativistic particles is also adiabatically compressed. Pressure equilibrium between the thermal gas and relativistic electrons gives a compression factor of $Y = X^{5/4}$, due to the ratio of adiabatic index of thermal gas and relativistic electrons (and also magnetic fields) of $\frac{5}{3}/\frac{4}{3}$. An electron increases its momentum during compression by a factor $Y^{1/3}$, so that a power law distribution with differential number index α_e gets an increased normalization by a factor $Y^{(2+\alpha_e)/3} = X^{5(2+\alpha_e)/12}$. The volume averaged intensity of IC scattering of a homogeneous photon population around our model galaxy would be 1.34 times the background value, for $\alpha_e = 2.5$. But for photons emitted in the center, which have an r^{-2} density profile, and are therefore most abundant at the location of highest electron densities, the volume averaged IC scattering for the compressed relativistic electrons is 4.8 times the value the same photon density profile would produce with a homogeneous electron profile.

References

- Abramowitz M., Stegun I.A., 1965, Handbook of Mathematical Functions. Dover, New York
- Biviano A., Durret F., Gerbal D., et. al., 1996, A&A 311, 95
- Bowyer S., Lampton M., Lieu R., 1996, Science 274, 1338
- Bowyer S., Lieu R., Mittaz J.P., 1997, IAU Symposium No. 188: The Hot Universe, 52
- Bowyer S., Berghöfer T.W., 1998, ApJ 506, 502
- Blumenthal G.R., Gould R.J., 1970, Rev. Mod. Phys. 42, 237
- Briel U.G., Henry J.P., Böhringer H., 1992, A&A 259, L31
- Brunetti G., Setti G., Comastri A., 1997, A&A 325, 898
- Burns J.O., Roettiger K., Pinkney J., Perley R.A., Owen F.N., 1995, ApJ 446, 583
- Colless M., Dunn A.M., 1996, ApJ 458, 435
- Crusius A.R., Schlickeiser R., 1986, A&A 164, L16
- Crusius-Wätzell A.R., Biermann P.L., Schlickeiser R., Lerche, I., 1990, ApJ 360, 417
- Dub, P.A., Laha, A., 1999, A. J. 284, 451

- Enßlin T.A., Biermann P.L., Kronberg P.P., Wu X.-P., 1997, *ApJ* 477, 560
- Enßlin T.A., Biermann P.L., 1998, *A&A* 330, 90
- Enßlin T.A., Wang Y., Nath B.B., Biermann P.L., 1998, *A&A* 333, L47
- Feretti L., Dallacasa D., Giovannini G., Tagliana A., 1995, *A&A* 302, 680
- Fusco-Femiano R., Fiume D. Dal, Feretti L., et al., 1998, Proceedings of '32nd COSPAR Scientific Assembly', Nagoya, Japan, in press, astro-ph/9808012
- Fusco-Femiano R., Fiume D. Dal, Feretti L., et al., 1999, *ApJL*, in press, astro-ph/9901018
- Giovannini G., Feretti L., Venturi T., Kim K.-T., Kronberg P.P., 1993, *ApJ* 406, 399
- Girardi M., Biviano A., Giuricin G., Mardirossian F., Mezzetti M., 1995, *ApJ* 438, 527
- Gregg M.D., West M.J., 1998, *Nature* 396, 549
- Haug E., 1997, *A&A* 326, 417
- Hughes J.P., Butcher J.A., Stewart G.C., Tanaka Y., *ApJ* 404, 619
- Hwang C.-Y., 1997, *Science* 278, 1917
- Kardashev N.S., 1962, *Sov. Astron. AJ* 6, 317
- Kim K.-T., Kronberg P.P., Dewdney P.E., Landecker T.L., 1990, *ApJ* 355, 29
- Kronberg P.P., Lesch H., Hopp U., 1999, *ApJ* 511, in press
- Lazzati D., Chincarini G., 1998, *A&A* 339, 52
- Lieu R., Mittaz J.P.D., Bowyer S., et al., 1996a, *Science* 274, 1335
- Lieu R., Mittaz J.P.D., Bowyer S., et al., 1996b, *ApJ* 458, L5
- Lieu R., Ip W.-H., Axford W.I., Bonamente M., 1999, *ApJ* 510, 25
- Loeb A., Mao S., 1994, *ApJ* 435, L109
- Melnick J., White S.D.M., Hoessel J., 1977, *MNRAS* 180, 207
- Miralda-Escudé J., Babul A., 1995, *ApJ* 449, 18
- Mittaz J.P.D., Lieu R., Lockman F.J., 1998, *ApJ* 498, L17
- Rephaeli Y., 1979, *ApJ* 227, 364
- Rephaeli Y., Ulmer M., Gruber D., 1994, *ApJ* 429, 554
- Sarazin C.L., Lieu R., 1998, *ApJ* 494, 177
- Secker J., Harris W.E., 1996, *ApJ* 469, 623
- Schlickeiser R., 1984, *A&A* 136, 227
- Strom K.M., Strom S.E., 1978, *AJ* 83, 73
- Spitzer L., 1968, *Diffuse Matter in Space*, John Wiley & Son, New York (1968)
- Thuan T.X., Kormendy J., 1977, *PASP* 89, 466
- Vikhlinin A., Forman W., Jones C., 1997, *ApJ* 474, L7
- Völk H. J., Aharonian F. A., Breitschwerdt D., 1996, *Space Sci. Rev.* 75, 279
- Völk H. J., Atoyan A.M., 1998, *Astroparticle Physics*, submitted, astro-ph/9812458
- Webbink R.F., Jeffers W.Q., 1969, *Space Sci. Rev.* 10, 191
- Willson M.A.G., 1970, *MNRAS* 151, 1